Vol. 24 • No. 17 • May 2 • 2014

www.afm-journal.de

ADVANCED FUNCTIONAL MATERIALS

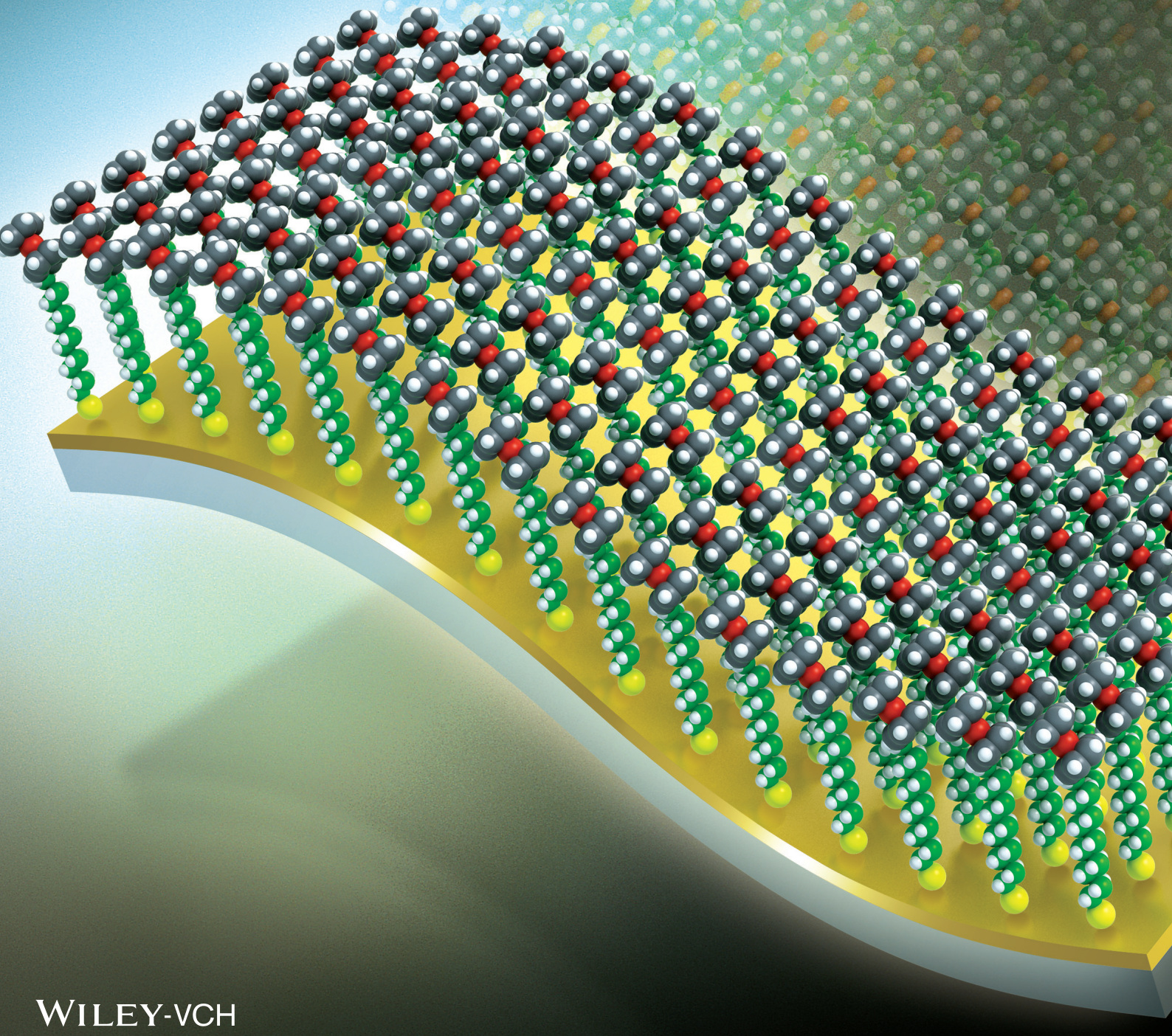

WILEY-VCH

ADVANCED FUNCTIONAL MATERIALS
www.afm-journal.de

Redox-Induced Asymmetric Electrical Characteristics of Ferrocene-Alkanethiolate Molecular Devices on Rigid and Flexible Substrates

Hyunhak Jeong, Dongku Kim, Gunuk Wang, Sungjun Park, Hanki Lee, Kyungjune Cho, Wang-Taek Hwang, Myung-Han Yoon, Yun Hee Jang, Hyunwook Song, Dong Xiang, and Takhee Lee**

The electrical properties of ferrocene-alkanethiolate self-assembled monolayers (SAMs) on a high yield solid-state device structure are investigated. The devices are fabricated using a conductive polymer interlayer between the top electrode and the SAM on both silicon-based rigid substrates and plastic-based flexible substrates. Asymmetric electrical transport characteristics that originate from the ferrocene moieties are observed. In particular, a distinctive temperature dependence of the current (i.e., a decrease in current density as temperature increases) at a large reverse bias, which is associated with the redox reaction of ferrocene groups in the molecular junction, is found. It is further demonstrated that the molecular devices can function on flexible substrates under various mechanical stress configurations with consistent electrical characteristics. This study enhances the understanding of asymmetric molecules and may lead to the development of functional molecular electronic devices on both rigid and flexible substrates.

1. Introduction

The study of molecular electronic devices that utilize single molecules or molecular monolayers as active electronic channels is important in understanding the electronic transport properties of molecules and developing miniaturized electronic devices for real-world applications.[1–3] Significant progress has been made towards understanding the charge transport characteristics of various molecular systems,[4–7] and molecular junctions displaying unique electrical properties have been investigated for use in a wide range of applications including diodes, switches, memory, and transistors.[8–14] However, many challenges remain in making molecular electronics a viable technology.

A primary obstacle in the development of molecular electronics is the lack of an accurate understanding of molecular reactions in the active electronic channels. For example, recently various types of molecular reactions such as change of chemical bonding, redox process, photo- or charge-induced conformational change, phase transition in molecular electronic devices have been widely investigated in order to enlarge the knowledge of intrinsic molecular properties.[12,15–21] However, these kinds of molecular reactions in molecular electronic devices are subjects still under debate due to a difficulty of precise characterizations. The absence of reliable and high-yield device platforms for testing molecular junctions that exhibit the unique and intrinsic functional properties of their component molecules is also one of the most common issues. In this context, various reliable and high-yield device platforms which utilize various types of materials such as graphene, PEDOT:PSS ((poly-(3,4-ethylenedioxythiophene) stabilized with poly-(4-styrenesulfonic acid)) are proposed and investigated even under unconventional environments.[22–25]

Here, we report the distinctive electrical characteristics of molecular junctions composed of ferrocene-alkanethiolate functional molecules as a solid-state device structure. The devices were fabricated using the conductive polymer PEDOT:PSS as a conducting interlayer electrode.[12,22,23] Interestingly, we observed a distinctive temperature dependence of the junction current density; that is, the current decreased with increasing temperature at temperatures with a threshold bias voltage upon an applied bias polarity. This is in contrast to the typical behavior for thermally activated charge transport, in which

H. Jeong, D. Kim, H. Lee, K. Cho, W.-T. Hwang, Dr. D. Xiang, Prof. T. Lee
Department of Physics and Astronomy
Seoul National University
Seoul 151–747, Korea
E-mail: xiangdongde@126.com; tlee@snu.ac.kr
Dr. G. Wang
Department of Chemistry and the Smalley Institute for Nanoscale Science and Technology
Rice University
Houston, TX 77005, USA
S. Park, Prof. M.-H. Yoon, Prof. Y. H. Jang
School of Material Science and Engineering
Gwangju Institute of Science and Technology
Gwangju 500–712, Korea
Prof. H. Song
Department of Applied Physics
Kyung Hee University
Yongin-si, Gyeonggi-do 446–701, Korea

DOI: 10.1002/adfm.201303591

© 2013 WILEY-VCH Verlag GmbH & Co. KGaA, Weinheim

current increases with increasing temperature. We propose that this unique behavior can be attributed to the redox process of ferrocene groups in the molecular junctions. In addition, we demonstrated that the working molecular devices could be fabricated on flexible substrates as well, exhibiting consistent conduction properties as rigid substrates even under severely bent conditions. This study suggests the understanding of the intrinsic molecular reactions is important when we apply functional molecules to molecular and organic electronic devices. Furthermore this study will lead to the further development of functional molecular electronic devices with flexible configurations.

2. Results and Discussion

Figure 1a depicts a schematic of the fabrication procedure for the molecular devices developed in this study. First, the bottom electrode was prepared by photolithography. A film of Au (50 nm) and Cr (10 nm) was deposited using an e-beam evaporator at a slow deposition rate of ≈0.1 Å s^{-1} to obtain a smooth electrode surface. The root mean square (RMS) roughness of the Au electrode surface was determined to be ≈0.19 nm using atomic force microscopy (AFM) images with a scan size of 1 μm × 1 μm (Figure S3 in the Supporting Information). Following film formation, self-assembled monolayers (SAMs) composed of an alkanethiol with a terminal ferrocene moiety were allowed to assemble on the film surface. Three molecules were used in this study: 6-ferrocenyl-1-hexanethiol (FcC6), 8-ferrocenyl-1-octanethiol (FcC8), and 11-ferrocenyl-1-undecanethiol (FcC11). The chemical structures of the molecules are shown in Figure 1c. The molecules varied in length depending on the number of alkyl chains present ($(CH_2)N$, where N = 6, 8, and 11; FcC6 and FcC11 are available from Sigma-Aldrich Co. and FcC8 is available from Dojindo Molecular Technologies, Inc.). The electrical characteristics of alkanethiol molecular junctions have been widely studied, and tunneling has been demonstrated as the main conduction mechanism.[13,22,24,26–34] When a ferrocene moiety was attached to the end of these alkanethiols, the overall molecular junctions exhibited an asymmetric electrical characteristics.[14,35–39] Due to its attractive property of the molecules, there have been many studies to investigate the characteristics of the molecular system. For example, an odd/even effect caused by the chain length of the alkyl chain of the alkanethiolates or ferrocene-alkanethiolates using the eutectic Ga and In (EGaIn)-electrode molecular junction platform was reported.[38,59] In our study, SAMs were deposited by immersing the samples for 1–2 days in a dilute ethanolic solution of the desired molecule in a N_2-filled glove box. The thiol moieties bond strongly to the bottom electrode (Au surface), while the ferrocene moieties make contact with the top electrode.

The previously reported vertical metal–molecule–metal junctions are prone to electrical shorting due to the penetration of the top metal through the SAM during metal evaporation, which creates conducting paths between the bottom and top electrodes.[32,40–43] To prevent electrical shorting, an intermediate protective layer such as a conducting polymer[22,25,44] or graphene film[24,45] can be introduced between the top electrode and the SAM. In our study, we used a method reported by Akkerman et al. in which a highly conductive polymer, PEDOT:PSS, was used as a conducting interlayer.[22,25] This fabrication technique was used to enhance the device yield,[46] and the reliability of molecular-scale electronic devices under mechanically deformed configurations was also

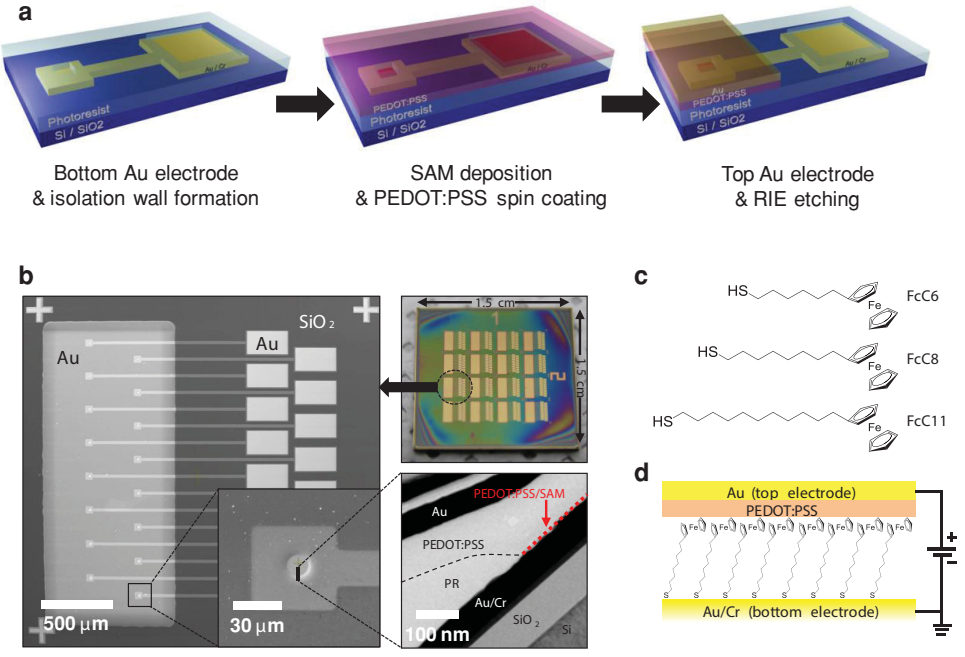

Figure 1. a) The molecular device fabrication processes on a rigid substrate. b) Optical, SEM, and cross-sectional TEM images of the molecular devices. The molecular junctions are circular with radii of 7, 8, and 9 μm. c) The chemical structures of the molecules. d) The schematic of the molecular device measurement setup.

© 2013 WILEY-VCH Verlag GmbH & Co. KGaA, Weinheim

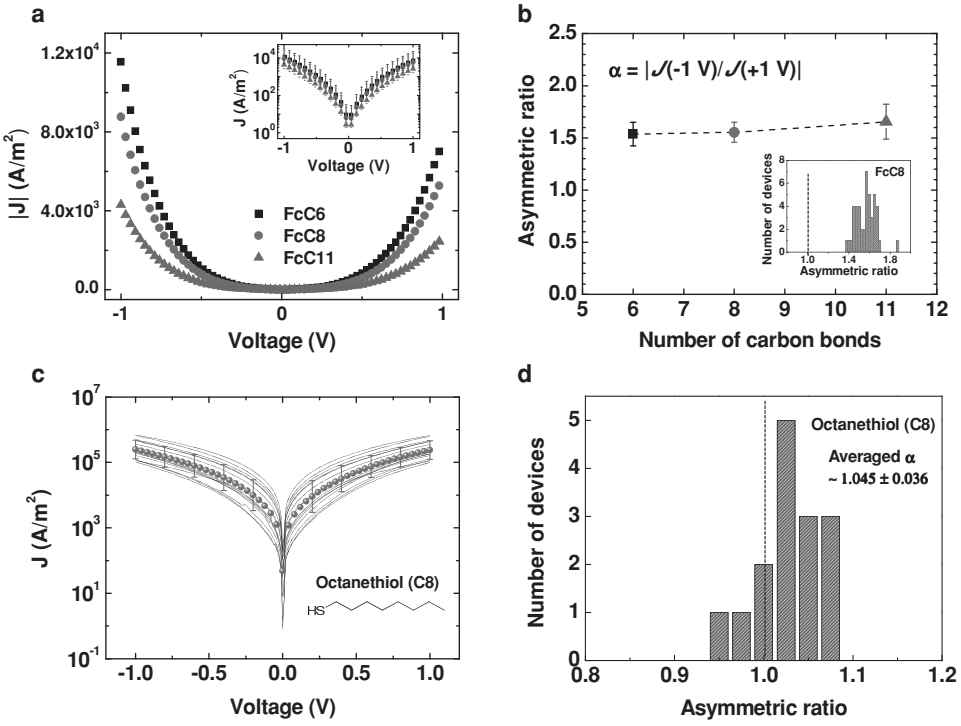

Figure 2. a) *J–V* characteristics for FcC6, FcC8, and FcC11 molecular devices. The inset shows a semi-log plot of the *J–V* characteristics with error bars determined from the standard deviation of all the measured devices (140 devices). b) Asymmetric ratio for FcC6, FcC8, and FcC11 molecular devices. Inset shows the histograms of the asymmetric ratios for FcC8. c) The *J–V* characteristics of Au/PEDOT: PSS/octanethiol (C8)/Au junctions. d) Histogram of asymmetric ratios for C8 devices.

demonstrated.[25] In this study, prior to depositing the top electrode, we spin-coated a PEDOT:PSS interlayer of 100 nm thickness, as determined using cross-sectional transmission electron microscopy (TEM) (Figure 1b). Subsequently, a 50 nm Au film was deposited on the PEDOT:PSS layer (Figure 1d). By using this PEDOT:PSS-interlayer fabrication method, we improved the device yield to near ≈50% (see Table S1 of the Supporting Information). In comparison, the device yield of simple metal-molecule-metal junctions without interlayers is typically ≈1%.[32,47] Approximately 100 molecular devices were fabricated on a single substrate (1.5 cm × 1.5 cm). The junctions were circular, with radii of 7, 8, and 9 μm. Scanning electron microscopy (SEM), TEM, and optical microscopy images of the fabricated devices are shown in Figure 1b. In addition, the device fabrication procedure is explained in detail in the Experimental Section and Supporting Information (Figure S1).

Figure 2a shows the representative current density-voltage (*J–V*) behavior of the three molecules of varying length used in our study. In this plot, the current density values at negative a bias were converted to positive values for easy comparison with those at a positive bias. The inset plot displays statistical *J–V* data from ≈50 measured devices for each molecular length. The error bars depict the standard deviation of the current density values measured from all of the working devices (≈140 devices, see Table S1 in the Supporting Information). Alkyl molecules with ferrocene moieties have previously exhibited asymmetric electrical properties, in which SAMs of these molecules were sandwiched between a Ag bottom electrode and a top electrode comprising eutectic Ga and In (EGaIn).[14,35–38] In this structure, rectification occurred because the highest occupied molecular orbital (HOMO) of the ferrocene moiety participated in charge transport under negative bias only. At a negative bias, the HOMO of ferrocene is located between the Fermi levels of the two electrodes and contributes to charge transport, whereas at a positive bias the HOMO of ferrocene is below the Fermi levels of both electrodes and therefore cannot contribute to charge transport.[35,37] We observed similar asymmetric electrical characteristics in our study but with somewhat lower asymmetric ratios. The asymmetric ratio (α), which is defined as $\alpha = |J(-1\text{ V})/J(1\text{ V})|$, where $J(\pm 1\text{ V})$ is the current density measured at ±1 V, was lower (α = ≈1.6) in our study. The summarized asymmetric ratios for different molecules are presented in Figure 2b with the statistical histogram of distribution in the inset. The observed low asymmetric ratio is due to the different junction structures employed, particularly for the top electrode material. The greater detail regarding the origin of this effect and conditions for improvement of the asymmetric ratio is explained in below (**Figure 3**d). And to ensure that the off unity asymmetric ratio is truly attributed to the ferrocene moiety, we could find from our previous reports that the estimated asymmetric ratio is clearly ≈1 when the deposited molecules are lacking the ferrocene moiety but under same device configurations.[25,46] Also from our freshly characterized results, we confirmed that similar tendency was repeatedly observed (Figure 2c,d). Therefore, the off unity asymmetric ratio evidently originates from the ferrocene moiety. And unlike the previous report by Nerngchamnong et al.,[38] we did not observe the odd/even effect in the asymmetric ratio using

© 2013 WILEY-VCH Verlag GmbH & Co. KGaA, Weinheim

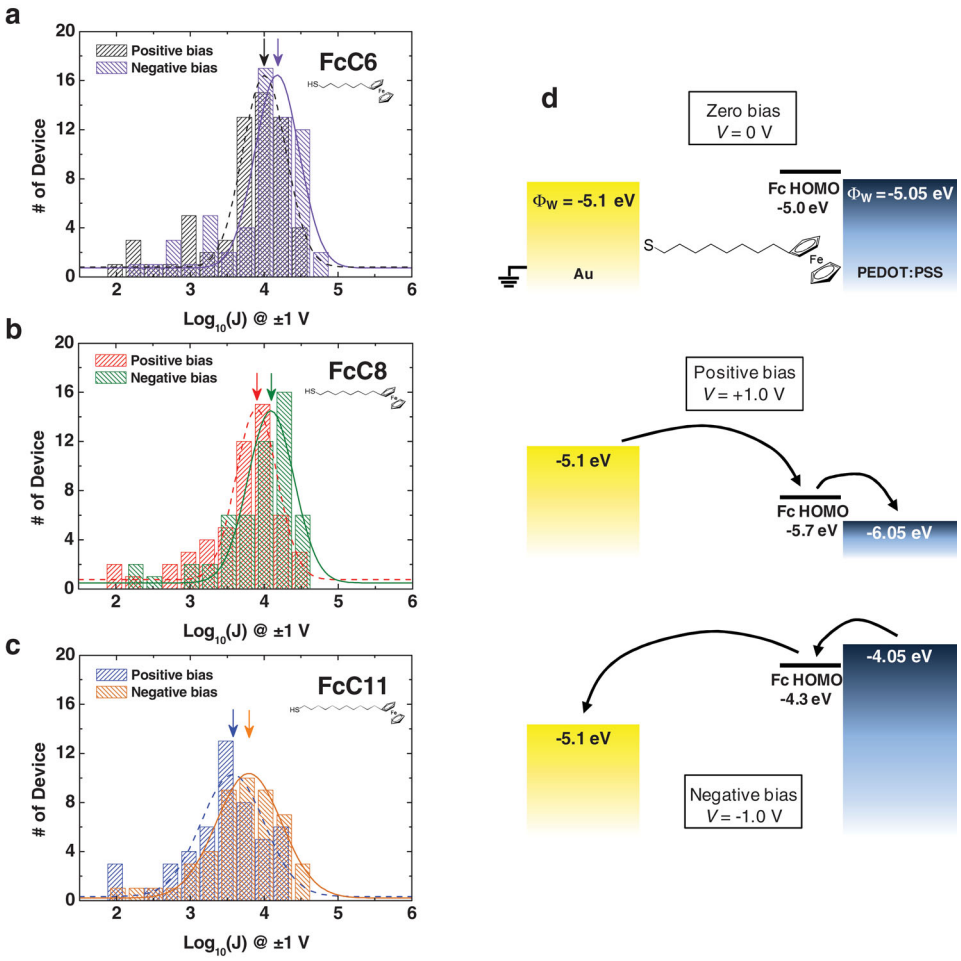

Figure 3. a,b,c) Histograms of the logarithmic current densities measured at ±1 V for FcC6, FcC8, and FcC11 molecular devices. The arrows indicate the mean value of the logarithmic current density of the each molecular device at both bias polarities. d) The proposed energy band diagram for the molecular junctions at three bias conditions (0, 1, and –1 V). Arrows depict the charge conduction through the molecular junction. The HOMO of ferrocene and the Fermi level of Au were adopted from the literature, while the Fermi level of PEDOT:PSS was measured by Kelvin Probe measurements.

three different lengths of ferrocene-alkanethiolates (FcC*n*, *n* = 6, 8, 11). We think that the absence of the odd/even effect in this study is caused by un-flatness of the bottom electrodes and the non-uniform contact between ferrocene moieties and the PEDOT:PSS interlayer.

Figure 3a–c depict the statistical histograms of the distribution of logarithmic current densities measured at ±1 V for our FcC6, FcC8, and FcC11 molecular devices. The arrows indicate representative values of each molecular devices. The logarithmic distribution of current density arises from variations in the linear distance between the top and bottom electrodes because the overall current, and the tunneling current in particular, depends exponentially on the gap distance between the two electrodes.[32,48] From this histogram, one can see that our devices exhibit asymmetric electrical characteristics, with the current at a negative bias (forward bias) statistically higher than that at a positive bias (reverse bias), which is regardless of molecular length.

To understand the origin of asymmetric electrical characteristics, Figure 3d shows the energy band diagrams of our molecular junctions. The work function of Au is ≈5.1 eV. The work function of PEDOT:PSS was determined to be ≈5.05 eV using a Kelvin probe measurement. The HOMO of the ferrocene moiety is ≈ –5.0 eV (i.e., 5.0 V below the vacuum level).[14,35–38] With these values, the energy band diagram at zero bias can be depicted as shown in the top schematic in Figure 3d. The middle and bottom schematics depict the energy band diagram when +1 V and –1 V are applied to the PEDOT:PSS side, respectively. For these diagrams we assumed that the ferrocene moiety formed van der Waals contacts with the PEDOT:PSS, resulting in a potential drop of 0.3 V, as described in previous reports.[14,35–38] Therefore, when +1 V is applied the HOMO of ferrocene decreases to –5.7 eV, whereas an applied bias of –1 V increases the HOMO to –4.3 eV. To achieve a high asymmetric ratio, the HOMO of the ferrocene moiety should lie between the Fermi levels of the two electrodes under one bias polarity (forward bias) but lie below the Fermi levels of both electrodes at the other bias polarity (reverse bias). These conditions enable a high asymmetric ratio because a HOMO that lies between the Fermi levels at the forward bias condition can act as a resonant energy

© 2013 WILEY-VCH Verlag GmbH & Co. KGaA, Weinheim

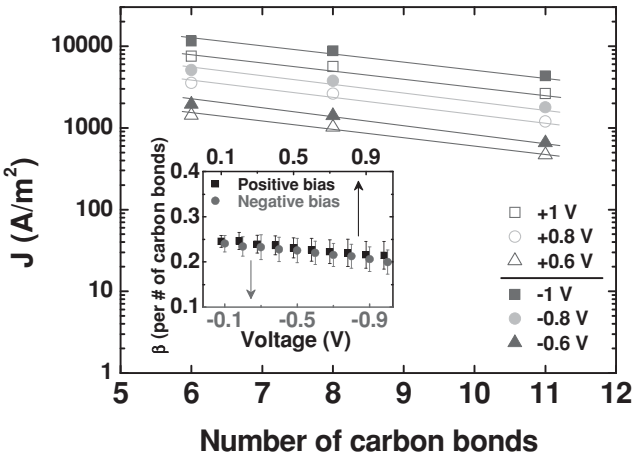

Figure 4. A semi-log plot of the current density as a function of the number of carbon bonds (i.e., the length of the alkyl chains). The lines through the data points represent the exponential fits. The inset displays the estimated decay coefficients at each bias.

state for charge transport.[14,35–39] However, in our study, the HOMO of ferrocene is located between the Fermi levels of each electrode (PEDOT:PSS and Au) at both bias polarities. Thus, the HOMO of the ferrocene can participate in charge transport at both bias polarity conditions, resulting in the low asymmetric ratio (~1.6) observed in our study (Figure 2b, and below).

As depicted in Figure 2a, the current density of each molecule decreases as the number of alkyl chains increases (N = 6, 8, 11). Longer molecular lengths lead to larger effective tunneling barrier widths, which results in a decrease in the tunneling current that displays an exponential dependence described by $J \propto \exp(-\beta d)$ (**Figure 4**), where β is the decay coefficient and d is the gap distance. The decay coefficient β can be deduced from the slope of the linear fitting of current density along the number of carbon bonds at a fixed bias, which obeys the exponential dependence as $J \propto \exp(-\beta d)$. The determined β values are shown in the inset of Figure 4. The β values were found to range from 0.20 to 0.25 per carbon bond for both positive and negative biases. The β values observed in our study are smaller than those previously reported for alkyl molecular junctions (0.7–1.2 per carbon bond).[24,27,29,30,32,60–63] We previously reported the β values of pure alkyl molecules to be ≈1.0 per carbon bond (corresponding to ≈0.8 Å^{-1}), which differs from the lower values for ferrocene-alkanethiolate molecules in our current study.[32,47,64]

To understand the electronic transport properties of our molecular junctions, we performed temperature-variable current–voltage (I–V–T) measurements while the temperature was varied from 80 to 300 K in increments of 20 K. **Figure 5**a,b present Arrhenius plots (ln(J) versus 1/T) of a FcC11 device at negative and positive bias, respectively (see Figure S4 in the Supporting Information for FcC6 and FcC8 devices). The currents were nearly bias-independent at lower temperatures, indicating that tunneling is the dominant conduction mechanism at this temperature range. However, at high temperatures (> ≈220 K), there is a distinction in the behavior between the two bias polarities. At a negative bias, weak thermal activation occurs at the high temperature range (Figure 5a). This

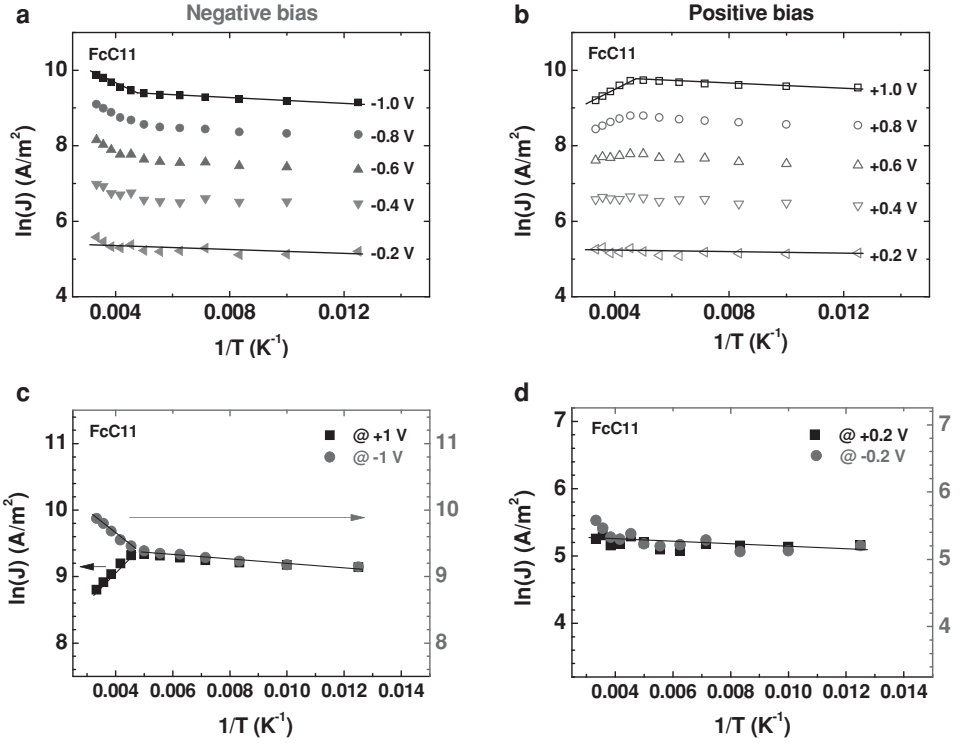

Figure 5. a,b) Arrhenius plots of ln(J) versus 1/T for an FcC11 molecular device at different a) negative and b) positive biases. c,d) Arrhenius plot of the data measured at c) ±1 V and d) ±0.2 V from plot (a) and (b), respectively.

© 2013 WILEY-VCH Verlag GmbH & Co. KGaA, Weinheim

thermal activation could be interpreted as weak hopping conduction (not thermionic conduction, detailed analysis is not provided here). More importantly, an interesting feature was observed at the positive bias polarity. As shown in Figure 5b, at the low temperature range the conduction is dominated by tunneling. However, at the high temperature range (> ≈220 K) and at high biases (e.g., the 0.6, 0.8, and 1.0 V conditions in Figure 5b), the current decreased with increasing temperature. Normally, current through a molecular junction (or other types of junctions) is either independent of temperature when a tunneling is dominating, or dependent on temperature such a way that current increases as the increasing temperature when a thermionic conduction or defect-mediate conduction mechanisms are dominating. On the contrary, we observed an opposite temperature dependent conduction characteristics in our study, which is that current decreased as the increasing temperature.

This unique feature, in which current decreases with increasing temperature at a positive bias, can be more clearly observed when the currents measured at ±1 V are plotted together as a function of temperature, as shown in Figure 5c. We can deduce that this feature is a molecular effect because typical metallic behavior was observed over the entire temperature range (i.e., current decreased with increasing temperature) for molecule-free Au/PEDOT:PSS/Au junctions, without the appearance of any unusual behavior at 220 K (see Figure S2b in the Supporting Information). Note that this unique feature was observed only at high positive biases (higher than ≈0.6 V) and did not occur at low positive biases (see Figure 5b,d and Figures S4–S6 in the Supporting Information). Combining these *I–V–T* results, we also plotted the asymmetric ratios as a function of temperature, as shown in Figures S6,S7 in the Supporting Information. At temperatures of up to ≈220 K, the asymmetric ratio was nearly constant. At higher temperatures (> ≈220 K), the asymmetric ratio increased due to the different *I–V–T* behaviors at negative and positive biases. This unique behavior was consistently observed for many of the other devices, regardless of molecule length (see Figures S6,S7 in the Supporting Information). Figure S7 in the Supporting Information describes six different devices for each molecular length (total of 18 devices), all of which exhibited similar behaviors.

One possible mechanism for our observation can be the redox-induced conformational change of ferrocene-alkanethiolate.[49] It has also been reported that the environmental effects such as surface coverage can make an influence on the orientation change by theoretical and experimental studies.[56–58] From reports in the literature,[56–58] we can expect that the orientation change of the ferrocene-alkanethiolates can be induced by the redox process of the ferrocene moieties. Ferrocene-alkanethiolate can be reversibly oxidized under relatively small applied biases due to the presence of strongly electron-donating ferrocene terminal groups,[50] whose oxidation peaks have been observed near +0.6 V with respect to a Au electrode using cyclic voltammetry.[49,51] Even in solid state junctions, this kind of redox process is shown to be available due to the charge injection to a special molecule with relevant molecular orbitals and metal complexes.[52–55] When ferrocenes are oxidized (to ferricenium cations) by applied biases higher than ≈+0.6 V, the positively charged ferrocene terminal groups in the SAM will exert a lateral repulsive force on the neighboring molecules.[49] This repulsion can be alleviated by increasing the distance between the oxidized ferrocenes. One way to achieve this is to orient the molecules perpendicular to the electrode surface,[49] leading to an increase in the distance between the two electrodes and a decrease in the current density between them. This type of SAM rearrangement would require an energy input, and a current density dependence on orientation would therefore appear at high temperatures (> ≈220 K in this work). But to understand the influence of the temperature on the distinctive electrical characteristics precisely, it is expected that the more delicate study should be progressed. From our data in Figure 5c and the estimated decay coefficient (β) value from Figure 4, we estimated that the current decrease from 220 to 300 K corresponds to a change of ≈2 Å in the distance between the two electrodes. Another possible mechanism is disordering in the SAMs due to electrostatic repulsions between the oxidized ferrocene moieties. Disordering would prevent the ferrocene moieties from making good contact with the PEDOT:PSS layer and reduce the current. Indeed, the disordering of SAMs of ferrocene-alkanethiolate has been described in a previous report.[38] In our molecular junctions, both of these mechanisms may be at work. Even so, further evidence is needed to fully understand our observation. As a control group, when the molecules had no ferrocene moieties but only the alkyl chain, there were no distinctive behaviors in the electrical characteristics at different temperatures.[25] Therefore, the electroactive nature of the ferrocene moieties is truly the origin of the distinctive temperature dependent behaviors observed in this study. Note that the device cyclability was maintained under several measurements without losing its own characteristics. Also the temperature sweep direction (i.e., high temperature to low temperature and low temperature to high temperature) did not influence on the manifestation of the distinctive temperature dependency. We expect the reason for the stability in spite of the dynamic process is that the degree of configuration change of the monolayer is fairly small compared to the length of the molecules. Guojon et al. has reported that the molecular orientation change due to the oxidation of the ferrocene is mainly observed in the random system (i.e., ferrocene-alkanethiolates diluted with alkanethiolates) whereas it is less pronounced in the cluster system (i.e., pure ferrocene-alkanethiolates).[56] Interestingly, we also observed this unique feature in the molecular junctions on flexible substrate structures, as explained in the following.

The ferrocene-alkanethiolate SAMs were also fabricated and characterized on a flexible substrate. The device fabrication procedure was similar to that used for the rigid device (Figure 1 and Supporting Information Figure S1), with the exception of the use of a polyimide (PI) substrate (Neopulim L-3430 purchased from Mitsubishi Gas Chemical Co., Inc.). The junction area on the flexible devices measured 30 μm × 30 μm. **Figure 6**a presents the representative J–V characteristics of FcC6, FcC8, and FcC11 flexible molecular devices fabricated on PI substrates under flat conditions (defined as bending radius = ∞). The current densities of the flexible devices were similar to those of the rigid devices (Figure 2a) within the error bar range. The asymmetric ratios (shown in the inset of Figure 6a) were also similar

© 2013 WILEY-VCH Verlag GmbH & Co. KGaA, Weinheim

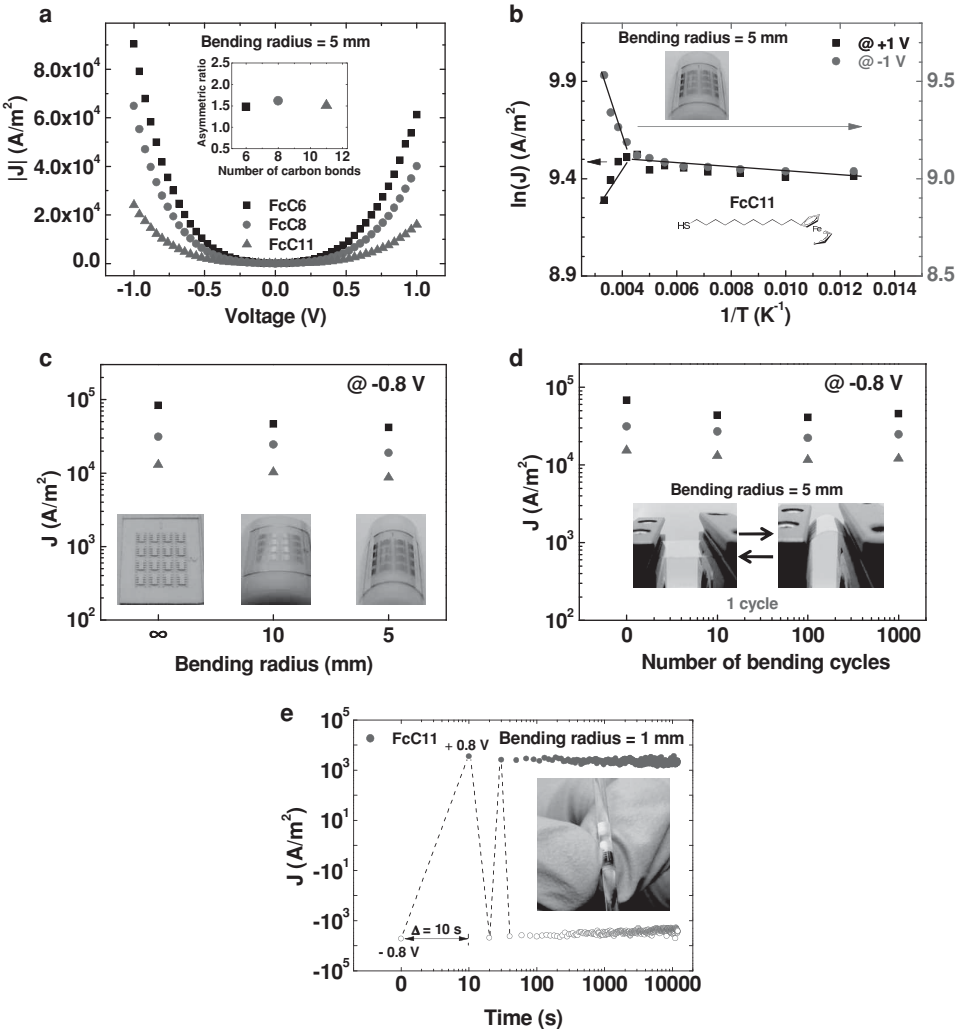

Figure 6. a) *J–V* characteristics of FcC6, FcC8, and FcC11 molecular devices fabricated on flexible substrates. The data were measured under bending conditions with a bending radius of 5 mm. The inset displays the asymmetric ratios of the devices under the same bending conditions. b) Arrhenius plot for a flexible FcC11 molecular device under bending conditions with a bending radius of 5 mm. c) The current density (*J*) values measured at –0.8 V for FcC6, FcC8, and FcC11 flexible molecular devices under various bending radius conditions (∞, 10 mm, and 5 mm). d) The current density (*J*) values measured at –0.8 V for FcC6, FcC8, and FcC11 flexible molecular devices under repeated bending cycles (0, 10, 100, and 1000 times; bending radius = 5 mm). e) A retention plot showing that the measured *J* values at ±0.8 V for 10^4 s (time interval Δt = 10 s) of an FcC11 flexible molecular device under extreme bending conditions (a thin cylindrical glass rod with radius = 1 mm).

to those of the rigid devices (Figure 2b). Subsequently, we examined the mechanical stability of these flexible molecular devices under various bending conditions. Figure 6c shows the current densities measured for the FnC6, FnC8, and FnC11 flexible molecular devices under different bending radius conditions (bending radius = ∞, 10 mm, and 5 mm). Figure 6d presents the current densities for these flexible devices after repeated bending cycles (10, 100, and 1000 times) at a bending radius of 5 mm. These results demonstrate that the electrical properties of our flexible molecular devices were well preserved under various mechanical bending conditions. The flexible devices were also tested under severe bending conditions with a bending radius of 1 mm, yet still maintained their electrical characteristics, as shown in Figure 6e. We further performed *I–V–T* measurements for our flexible molecular devices under a bent configuration with a bending radius of 5 mm, and the results are shown in Figure 6b. The unique feature (the decrease of current with increasing temperature at positive biases) that was observed for the rigid devices (Figure 5c and Figure S6 in the Supporting Information) was also observed in the flexible devices under a bent configuration, confirming that this characteristic is reproducible in both rigid and flexible devices and under both flat and bending conditions. This results represent the distinctive electrical characteristics are intrinsic molecular properties irrelevant to external conditions such as substrate type or mechanical stress. Remarkably, our thin molecular layer devices on flexible substrates are able to maintain their molecular conductance characteristics under bending conditions due to the dominant through-bond pathways of molecular junctions.[25]

© 2013 WILEY-VCH Verlag GmbH & Co. KGaA, Weinheim

3. Conclusion

In summary, we studied the redox-induced electronic transport properties of ferrocene-alkanethiolate molecules using a conducting polymer-interlayer device structure. We observed asymmetric electrical transport properties, which arise due to the existence of ferrocene moiety. In particular, we observed distinctive electrical characteristics that the current in the junction decreased with increasing temperature at high temperatures (> ≈220 K) and when a large positive bias (> ≈0.6 V) was applied to the ferrocene end-group side. This behavior is attributed to the redox process of the ferrocene moiety in the molecular junction. We also fabricated the same molecular junctions on flexible device substrates and demonstrated consistent electrical characteristics (i.e., asymmetric current-voltage characteristics and distinctive temperature dependence) under various bending configurations. This ensures that the unique feature originated from the intrinsic molecular reactions but not from the effect of substrates or device configuration. Our study suggests the importance of consideration of intrinsic molecular reactions especially redox process when one applies molecules to the robust functional molecular devices. And this work also provides a route toward the practical implementation of functional molecular devices with unconventional flexible configurations.

4. Experimental Section

Fabrication of Rigid and Flexible Molecular Devices: The substrates used in this study were first prepared by general cleaning process with acetone, methanol, and deionized water. The patterned bottom Au (50 nm)/Cr (10 nm) electrodes generated by optical lithography or shadow mask technique and metal evaporation with e-beam evaporator were made on rigid (Si/SiO_2) or plastic (PI; Neopulim L-3430, purchased from Mitsubishi Gas Chemical Co. Inc.) substrates. Then, to create isolation wall, photoresist (Az5214E, purchased from Az Electronic Materials) was spin-coated (4000 rpm, 1 minute) on substrates and via-hole for SAMs was made. After that, in order to prevent the isolation wall from being soluble in SAM solution, the substrates were hard-baked with 190 °C for 2 h. Immediately, the substrates were dipped into the SAM solutions (≈3 mm in anhydrous ethanol) in N_2-filled glove box for 1–2 day. After deposition of SAMs, the substrates were rinsed with anhydrous ethanol and then dried by N_2 stream in N_2-filled glove box for ~2 h. Then, conducting polymer PEDOT:PSS (PH1000, purchased from Clevios) interlayer was spin-coated (3500 rpm, 30 s) on the substrates. After the coating, Au (50 nm) top electrodes were created. Finally, with reactive ion etching (RIE) process (using O_2 gas, 11 sccm, 60 mTorr, 50 W), residual PEDOT:PSS was removed.

Device Characterization: The electrical characteristics of the devices were measured with a semiconductor parameter analyzer (Keithley 4200 SCS) and a probe station system (JANIS Model ST-500).

Supporting Information

Supporting Information is available from the Wiley Online Library or from the author.

Acknowledgements

H.J. and D.K. contributed equally to this work. The authors appreciate financial support from the National Creative Research Laboratory program (Grant No. 2012026372) and the National Core Research Center program (Grant No. R15–2008–006–03002–0) through the National Research Foundation of Korea (NRF) funded by the Korean Ministry of Science, ICT & Future Planning. The authors also thank Dr. Y. H. Kahng and J.-H. Lee for their help on Kelvin probe measurements.

Received: October 22, 2013
Revised: October 28, 2013
Published online: December 20, 2013

[1] A. Aviram, M. A. Ratner, *Chem. Phys. Lett.* **1974**, *29*, 277.
[2] A. Nitzan, M. A. Ratner, *Science* **2003**, *300*, 1384.
[3] J. C. Cuevas, E. Scheer, *Molecular Electronics: An Introduction to Theory and Experiment*, World Scientific Publishing Co. Pte. Ltd., Singapore **2010**.
[4] M. A. Reed, C. Zhou, C. J. Muller, T. P. Burgin, J. M. Tour, *Science* **1997**, *278*, 252.
[5] L. Venkataraman, J. E. Klare, C. Nuckolls, M. S. Hybertsen, M. L. Steigerwald, *Nature* **2006**, *442*, 904.
[6] M. Galperin, M. A. Ratner, A. Nitzan, A. Troisi, *Science* **2008**, *319*, 1056.
[7] L. Lafferentz, F. Ample, H. Yu, S. Hecht, C. Joachim, L. Grill, *Science* **2009**, *323*, 1193.
[8] J. Chen, M. A. Reed, A. M. Rawlett, J. M. Tour, *Science* **1999**, *286*, 1550.
[9] W. J. Liang, M. P. Shores, M. Bockrath, J. R. Long, H. Park, *Nature* **2002**, *417*, 725.
[10] J. Park, A. N. Pasupathy, J. I. Goldsmith, C. Chang, Y. Yaish, J. R. Petta, M. Rinkoski, J. P. Sethna, H. D. Abruna, P. L. McEuen, D. C. Ralph, *Nature* **2002**, *417*, 722.
[11] J. E. Green, J. W. Choi, A. Boukai, Y. Bunimovich, E. Johnston-Halperin, E. DeIonno, Y. Luo, B. A. Sheriff, K. Xu, Y. S. Shin, H. R. Tseng, J. F. Stoddart, J. R. Heath, *Nature* **2007**, *445*, 414.
[12] A. J. Kronemeijer, H. B. Akkerman, T. Kudernac, B. J. van Wees, B. L. Feringa, P. W. M. Blom, B. de Boer, *Adv. Mater.* **2008**, *20*, 1467.
[13] H. Song, Y. Kim, Y. H. Jang, H. Jeong, M. A. Reed, T. Lee, *Nature* **2009**, *462*, 1039.
[14] C. A. Nijhuis, W. F. Reus, A. C. Siegel, G. M. Whitesides, *J. Am. Chem. Soc.* **2011**, *133*, 15397.
[15] P. A. Derosa, S. Guda, J. M. Seminario, *J. Am. Chem. Soc.* **2003**, *125*, 14240.
[16] C. B. Gorman, R. L. Carroll, R. R. Fuierer, *Langmuir* **2001**, *17*, 6923.
[17] U. Jung, O. Filinova, S. Kuhn, D. Zargarani, C. Bornholdt, R. Herges, O. Magnussen, *Langmuir* **2010**, *26*, 13913.
[18] Y. Kim, T. J. Hellmuth, D. Sysoiev, F. Pauly, T. Pietsch, J. Wolf, A. Erbe, T. Huhn, U. Groth, U. E. Steiner, E. Scheer, *Nano Lett.* **2012**, *12*, 3736.
[19] R. McCreery, J. Dieringer, A. O. Solak, B. Snyder, A. M. Nowak, W. R. McGovern, S. DuVall, *J. Am. Chem. Soc.* **2003**, *125*, 10748.
[20] R. L. McCreery, J. Wu, R. P. Kalakodimi, *Phys. Chem. Chem. Phys.* **2006**, *8*, 2572.
[21] M. M. Russew, S. Hecht, *Adv. Mater.* **2010**, *22*, 3348.
[22] H. B. Akkerman, P. W. M. Blom, D. M. de Leeuw, B. de Boer, *Nature* **2006**, *441*, 69.
[23] P. A. Van Hal, E. C. P. Smits, T. C. T. Geuns, H. B. Akkerman, B. C. De Brito, S. Perissinotto, G. Lanzani, A. J. Kronemeijer, V. Geskin, J. Cornil, P. W. M. Blom, B. De Boer, D. M. De Leeuw, *Nat. Nanotechnol.* **2008**, *3*, 749.
[24] G. Wang, Y. Kim, M. Choe, T. W. Kim, T. Lee, *Adv. Mater.* **2011**, *23*, 755.
[25] S. Park, G. Wang, B. Cho, Y. Kim, S. Song, Y. Ji, M. H. Yoon, T. Lee, *Nat. Nanotechnol.* **2012**, *7*, 438.
[26] D. J. Wold, C. D. Frisbie, *J. Am. Chem. Soc.* **2001**, *123*, 5549.

© 2013 WILEY-VCH Verlag GmbH & Co. KGaA, Weinheim

[27] X. D. Cui, X. Zarate, J. Tomfohr, O. F. Sankey, A. Primak, A. L. Moore, T. A. Moore, D. Gust, G. Harris, S. M. Lindsay, *Nanotechnology* **2002**, *13*, 5.
[28] M. A. Rampi, G. M. Whitesides, *Chem. Phys.* **2002**, *281*, 373.
[29] W. Y. Wang, T. Lee, M. A. Reed, *Phys. Rev. B* **2003**, *68*, 035416.
[30] V. B. Engelkes, J. M. Beebe, C. D. Frisbie, *J. Am. Chem. Soc.* **2004**, *126*, 14287.
[31] W. Y. Wang, T. Lee, I. Kretzschmar, M. A. Reed, *Nano Lett.* **2004**, *4*, 643.
[32] T. W. Kim, G. N. Wang, H. Lee, T. Lee, *Nanotechnology* **2007**, *18*, 315204.
[33] J. M. Beebe, B. Kim, C. D. Frisbie, J. G. Kushmerick, *ACS Nano* **2008**, *2*, 827.
[34] Y. Kim, H. Song, F. Strigl, H. F. Pernau, T. Lee, E. Scheer, *Phys. Rev. Lett.* **2011**, *106*, 196804.
[35] C. A. Nijhuis, W. F. Reus, G. M. Whitesides, *J. Am. Chem. Soc.* **2009**, *131*, 17814.
[36] C. A. Nijhuis, W. F. Reus, J. R. Barber, M. D. Dickey, G. M. Whitesides, *Nano Lett.* **2010**, *10*, 3611.
[37] C. A. Nijhuis, W. F. Reus, G. M. Whitesides, *J. Am. Chem. Soc.* **2010**, *132*, 18386.
[38] N. Nerngchamnong, L. Yuan, D. C. Qi, J. Li, D. Thompson, C. A. Nijhuis, *Nat. Nanotechnol.* **2013**, *8*, 113.
[39] Y. Q. Liu, A. Offenhausser, D. Mayer, *Phys. Status Solidi A.* **2010**, *207*, 891.
[40] G. L. Fisher, A. V. Walker, A. E. Hooper, T. B. Tighe, K. B. Bahnck, H. T. Skriba, M. D. Reinard, B. C. Haynie, R. L. Opila, N. Winograd, D. L. Allara, *J. Am. Chem. Soc.* **2002**, *124*, 5528.
[41] B. de Boer, M. M. Frank, Y. J. Chabal, W. R. Jiang, E. Garfunkel, Z. Bao, *Langmuir* **2004**, *20*, 1539.
[42] A. V. Walker, T. B. Tighe, O. M. Cabarcos, M. D. Reinard, B. C. Haynie, S. Uppili, N. Winograd, D. L. Allara, *J. Am. Chem. Soc.* **2004**, *126*, 3954.
[43] H. Haick, D. Cahen, *Acc. Chem. Res.* **2008**, *41*, 359.
[44] A. B. Neuhausen, A. Hosseini, J. A. Sulpizio, C. E. D. Chidsey, *ACS Nano* **2012**, *6*, 9920.
[45] S. Seo, M. Min, J. Lee, T. Lee, S. Y. Choi, H. Lee, *Angew. Chem. Int. Edit.* **2012**, *51*, 108.
[46] G. Wang, H. Yoo, S. I. Na, T. W. Kim, B. Cho, D. Y. Kim, T. Lee, *Thin Solid Films* **2009**, *518*, 824.
[47] G. Wang, T. W. Kim, H. Lee, T. Lee, *Phys. Rev. B* **2007**, *76*, 205320.
[48] W. F. Reus, C. A. Nijhuis, J. R. Barber, M. M. Thuo, S. Tricard, G. M. Whitesides, *J. Phys. Chem. C* **2012**, *116*, 6714.
[49] S. Ye, Y. Sato, K. Uosaki, *Langmuir* **1997**, *13*, 3157.
[50] A. V. Tivanski, G. C. Walker, *J. Am. Chem. Soc.* **2005**, *127*, 7647.
[51] X. Y. Xiao, D. Brune, J. He, S. Lindsay, C. B. Gorman, N. J. Tao, *Chem. Phys.* **2006**, *326*, 138.
[52] A. Migliore, A. Nitzan, *ACS Nano* **2011**, *5*, 6669.
[53] C.-P. Chen, W.-R. Luo, C.-N. Chen, S.-M. Wu, S. Hsieh, C.-M. Chiang, T.-Y. Dong, *Langmuir* **2013**, *29*, 3106.
[54] K. Seo, A. V. Konchenko, J. Lee, G. S. Bang, H. Lee, *J. Mater. Chem.* **2009**, *19*, 7617.
[55] R. A. Kiehl, J. D. Le, P. Candra, R. C. Hoye, T. R. Hoye, *Appl. Phys. Lett.* **2006**, *88*, 172102.
[56] F. Goujon, C. Bonal, B. Limoges, P. Malfreyt, *J. Phys. Chem. B* **2010**, *114*, 6447.
[57] G. Filippini, Y. Israeli, F. Goujon, B. Limoges, C. Bonal, P. Malfreyt, *J. Phys. Chem. B* **2011**, *115*, 11678.
[58] L. Y. S. Lee, T. C. Sutherland, S. Rucareanu, R. B. Lennox, *Langmuir* **2006**, *22*, 4438.
[59] M. M. Thuo, W. F. Reus, C. A. Nijhuis, J. R. Barber, C. Kim, M. D. Schulz, G. M. Whitesides, *J. Am. Chem. Soc.* **2011**, *133*, 2962.
[60] X. D. Cui, A. Primak, X. Zarate, J. Tomfohr, O. F. Sankey, A. L. Moore, T. A. Moore, D. Gust, G. Harris, S. M. Lindsay, *Science* **2001**, *294*, 571.
[61] R. E. Holmlin, R. Haag, M. L. Chabinyc, R. F. Ismagilov, A. E. Cohen, A. Terfort, M. A. Rampi, G. M. Whitesides, *J. Am. Chem. Soc.* **2001**, *123*, 5075.
[62] D. J. Wold, R. Haag, M. A. Rampi, C. D. Frisbie, *J. Phys. Chem. B* **2002**, *106*, 2813.
[63] H. B. Akkerman, A. J. Kronemeijer, P. A. van Hal, D. M. de Leeuw, P. W. M. Blom, B. de Boer, *Small* **2008**, *4*, 100.
[64] H. Song, T. Lee, N. J. Choi, H. Lee, *J. Vac. Sci. Technol. B* **2008**, *26*, 904.

© 2013 WILEY-VCH Verlag GmbH & Co. KGaA, Weinheim